Institute of Space and Aeronautical Science, University of Tokyo
Report No. 539, March 1976

Starting-length Problem of Laminar Film Condensation**

By

Nobuhide NISHIKAWA*

Summary: The film condnsation in a laminar boundary layer flow is analyzed for the case of combined body force with forced convection. Introduction of the starting length parameter X_c enables us to formulate the problem without any specification for a flow model that film formation initiates at a certain point downstream of the leading edge; a non-wetted initial section exists over $0 \leqq x < X_c$. With the assumed various lengths of initial non-wetted region the boundary layer equations for a steam-air mixture have actually been computed by means of the finite difference schemes, for a wide variety of flow parameters: the uniform flow velocity, the mass fraction of steam and the bulk-to-wall temperature difference. The effect of initial non-wetted length on the heat transfer is examined. The results for the limiting case $X_c \to 0$ are estimated by extrapolation of the solutions for finite X_c's, and these are compared with the previous studies for the cases of mixed convection, and also the limiting case of body force only.

1. INTRODUCTION

The problem of laminar film condensation has been analyzed by many investigators. The characteristic features involved in the relevant flow phenomena have been clarified: the effect of the presence of non-condensable gas in a vapor on condensation heat transfer [*1*], [2], the effect of variable transport properties in gaseous and condensate layers [*1*], and so on. On taking into account these effect, recently Denny, Mills, and Jusionis [*3*] numerically analyzed the flow with laminar film condensation on a vertical surface by means of an implicit finite difference method, using a forward marching technique. In applying the forward marching technique, however the flow-variable profiles must primarily be specified at the leading edge, if both gas and liquid boundary layers are assumed to initiate just at the leading edge. Denny et al. assumed the initial profiles which are determined by a Couette-type analysis together with an approximate relation between the incoming momentum and shear stress at the interface [*3*].

In the present paper we are still concerned with a numerical analysis of laminar film condensation on a vertical surface. To the author's knowledge, all of the previous works concerned dealt with the flow along the surface wholly wetted from the leading edge. Here we suppose the flow model that

* Department of Mechanical Engineering, Faculty of Engineering, Chiba University.
** This work was done while the author was Kyodo-Kenkyuin (Cooperative research fellow) of Institute of Space and Aeronautical Science, University of Tokyo.

the surface is non-wetted over a leading section, so that the liquid film grows up from the rear end of this region toward downstream. Then the problem is treated under a varying wall condition with sudden change in both surface temperature and mass flux at film initiation point. The distance from the leading edge to the film initiation point is designated as the starting-length.

For the analysis of the problem above described, we should refer to the laminar boundary layer problems with stepwise variation in wall temperature or mass flux. This kind of problem was analyzed by Eckert [*4*], Lighthill [*5*], Scesa and Levy [*6*], Fox and Libby [*7*], and Cheng et al. [*8*]. Eckert, Scesa and Levy confirmed that the solution for cases of finite but small starting-length approaches closely the exact solution [9] for the case of constant surface temperature with vanishing starting-length. The similar result was obtained by Libby [*10*] for the boundary layer with stepwise variation in mass flux toward the surface.

In the present analysis, first we obtain the solutions for ceses of various lengths of the non-wetted leading section, and examine the effect of the length of the non-wetted section on the heat transfer. Moreover the solution for the case of vanishing non-wetted region or wholly wetted wall is estimated by extrapolation of the solutions for cases of finite starting-lengths.

2. Mathematical Formulation

2. 1 Physical model and basic assumptions

A schematic diagram of the physical model concerned is illustrated in Fig. 1; that is, the wall is assumed to be non-wetted from the leading edge down to a point $x^*=X_c^*$ and the liquid film initiates to grow at this point. The flow of vapor-gas mixture covers a condensate layer adjacent to a finite flat plate. The wall temperature T_w is held lower than the free stream temperature T_e which is assumed to take the saturation value at the free stream state. Suppose a plate placed vertically, then the liquid film flows down

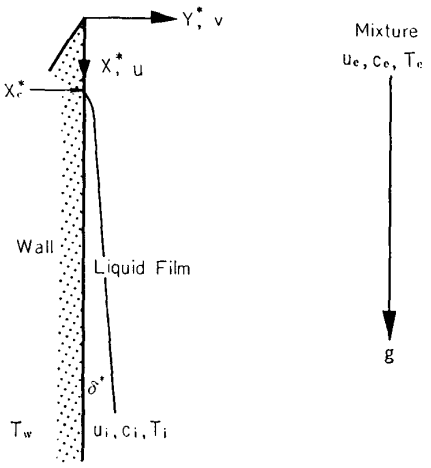

FIG, 1. Sehematic illustration of flow model.

due to both gravity and interfacial drag.

Prior to introduction of the governing equations the following assumptions are made;

1. Liquid flow through a condensate layer as well as vapor-gas mixture flow are laminar.
2. The radius of curvature of the film surface is sufficiently greater than the thickness of the gas-phase boundary layer.
3. In vapor-gas mixture the transport effect of thermal diffusion is negligible. The viscous dissipation as well as the work done by pressure are also ignored, because the free stream velocity u_e concerned is comparatively low.

2.2 Governing equations

It is convenient for the analysis of gas-phase boundary layer to choose the Cartesian coordinates (x^*, y^*), as illustrated in Fig. 1. The conservations of mass momentum, vapor species, and energy in the gas-phase boundary layer along the liquid film are written with the assumption of thin liquid layer as follows:

$$\frac{\partial(\rho u)}{\partial x^*}+\frac{\partial(\rho v)}{\partial y^*}=0, \tag{1}$$

$$\rho u\frac{\partial u}{\partial x^*}+\rho v\frac{\partial u}{\partial y^*}=\frac{\partial}{\partial y^*}\left(\mu\frac{\partial u}{\partial y^*}\right)+g(\rho-\rho_e), \tag{2}$$

$$\frac{\partial p}{\partial y^*}=0, \tag{3}$$

$$\rho u\frac{\partial c}{\partial x^*}+\rho v\frac{\partial c}{\partial y^*}=\frac{\partial}{\partial y^*}\left(\rho D\frac{\partial c}{\partial y^*}\right), \tag{4}$$

$$\rho C_p\left(u\frac{\partial T}{\partial x^*}+v\frac{\partial T}{\partial y^*}\right)=\frac{\partial}{\partial y^*}\left(k\frac{\partial T}{\partial y^*}\right)+\rho D(C_{p,v}-C_{p,g})\frac{\partial c}{\partial y^*}\frac{\partial T}{\partial y^*}. \tag{5}$$

In these equations u, v are the velocity components pertinent to the x^* and y^* coordinates, the symbols ρ, p, T, and c represent the density of the mixture, the total pressure of the mixture, the temperature, and the local mass fraction of the vapor, respectively, and g the gravitational acceralation. The viscosity, the thermal conductivity, and the binary diffusion coefficients are denoted by μ, k, and D, respectively, and the specific heat at constant pressure by C_p. The subscripts v and g refer to quantities pertinent to the vapor and the non-condensable gases, respectively, and the variables without these subscripts refer to the mixture. The subscript e refers to the free stream.

To enclose the problem the equation of state for gas mixture is required; here it is assumed that the mixture behaves like a perfect gas, i. e.

$$p=\rho RT, \tag{6}$$

where R is the gas constant for the mixture.

As for the liquid motion through the film the velocity is so small that the convective terms in the conservation equations can be neglected. Then we have

$$0=\mu_L\frac{d^2u}{dy^{*2}}+g(\rho_L-\rho_c), \tag{7}$$

$$0=k_L\frac{d^2T}{dy^{*2}}, \tag{8}$$

where the the subscript L refers to quantities pertinent to the liquid. These simplified equations were first proposed by Nusselt [*11*], being called Nusselt assumption.

2.3 Introduction of dimensionless quantities

For convenience the following dimensionless variables are introduced for the two-phase boundary layer; The spatial coordinates x^*, y^*, are non-dimensionalized by a reference length L;

$$x=x^*/L,\ y=y^*/L.$$

The ordinary boundary layer coordinates are introduced

$$\eta=\frac{u_e\int_0^{y^*}\rho dy^*}{\sqrt{2\rho_e\mu_e u_e x^*}}. \tag{9}$$

With the stream function defined by

$$\frac{\partial\psi}{\partial y^*}=\rho u,\quad \frac{\partial\psi}{\partial x^*}=-\rho v, \tag{10}$$

the dimensionless stream function f is introduced

$$f=\psi/\sqrt{2\rho_e\mu_e u_e x^*}. \tag{11}$$

If we use

$$U=u/u_e,\ \theta=T/T_e, \tag{12}$$

by the transformations (9)-(12) the basic equations (1)-(5) are rewritten

$$\frac{\partial}{\partial\eta}\left(\frac{\rho\mu}{\rho_e\mu_e}\frac{\partial U}{\partial\eta}\right)+f\frac{\partial U}{\partial\eta}=2x\left[U\frac{\partial U}{\partial x}-\frac{\partial f}{\partial x}\frac{\partial U}{\partial\eta}-G\left(1-\frac{\rho_e}{\rho}\right)\right], \tag{13}$$

$$\frac{\partial}{\partial\eta}\left(\frac{\rho^2D}{\rho_e\mu_e}\frac{\partial c}{\partial\eta}\right)+f\frac{\partial c}{\partial\eta}=2x\left(U\frac{\partial c}{\partial x}-\frac{\partial f}{\partial x}\frac{\partial c}{\partial\eta}\right), \tag{14}$$

$$\frac{k_e}{\mu_e C_p}\frac{\partial}{\partial\eta}\left(\frac{\rho k}{\rho_e k_e}\frac{\partial\theta}{\partial\eta}\right)+f\frac{\partial\theta}{\partial\eta}=2x\left(U\frac{\partial\theta}{\partial x}-\frac{\partial f}{\partial x}\frac{\partial\theta}{\partial\eta}\right)-\frac{\rho^2D}{\rho_e\mu_e}\frac{C_{p,v}-C_{p,g}}{C_p}\frac{\partial c}{\partial\eta}\frac{\partial\theta}{\partial\eta}, \tag{15}$$

where

$$G=gL/u_e^2$$

gives the magnitude of body force.

The equations (7) and (8) for the liquid layer are rewritten in the dimensionless forms:

$$\frac{d^2U}{dy^2}=-GR_e\frac{\mu_e}{\mu_L}\left(\frac{\rho_L}{\rho_e}-1\right),$$

$$\frac{d^2\theta}{dy^2}=0,$$

with the Reynolds number Re defined by

$$Re=\rho_e u_e L/\mu_e.$$

Assuming that ρ_L and μ_L vary in the streamwise direction but are constant across the film, we have the following solutions of Eq. (7) and Eq. (8), respectively.

$$U=-G\cdot Re\cdot Ay^2+\left(\frac{U_i}{\delta}+GReA\delta\right)y, \tag{16}$$

$$\theta=\theta_w+(\theta_i-\theta_w)\frac{y}{\delta}, \tag{17}$$

where

$$A=(\rho_L/\rho_e-1)\mu_e/2\mu_L.$$

In these equations δ is the nondimensional film thickness and the subscripts i and w refer to the quantities respectively at the interface and at the wall.

2.4 Boundary Conditions

Assuming that there is no slip at the wall and the wall temperature is fixed constant, we have the conditions:

$$y^*=0,\ u=0,\ T=T_w. \tag{18}$$

The external flow is assumed to be uniform, and then

$$y^*\to\infty,\ u\to u_e,\ T\to T_e,\ c\to c_e. \tag{19}$$

Once both T_e and c_e are given for saturated vapor, we can determine the mixture pressure p.

The film geomtry $\delta^*(x)$ is unknown prior to the solution. The following relations must be satisfied at the interface, regarding the velocity, the temperature, the shear stress, mass flux, and the heat flux.

$y^*=\delta^*(x)$;

$$u=u_L=u_i, \tag{20}$$

$$T=T_L=T_i, \tag{21}$$

shear stress balance:

$$\mu_i \frac{\partial u}{\partial y^*} = \mu_L \frac{du}{dy^*}, \tag{22}$$

mass flux continuity:

$$\frac{\rho D_i}{1-C_i} \frac{\partial c}{\partial y^*} = \frac{d}{dx^*} \int_0^{\delta^*} \rho_L u_L dy^* \equiv \dot{m}^*. \tag{23}$$

heat balance:

$$k_i \frac{\partial T}{\partial y^*} + \dot{m}^* h_L^* = k_L \frac{dT}{dy^*}, \tag{24}$$

where the subscript i refers to quantities pertinent to the interface, and $\dot{m}^*$ is the condensation rate per unit area and per unit time and h_L^* is the latent heat per unit mass.

The interface conditions above derived still contain four unknwns; δ^*, u_i, T_i, and c_i. In order to attain closure of the problem, we need one more constraint. We assume that the vapor in contact with the interface is saturated. If the mixture and its components behave like perfect gases, than the vapor mass fraction c_i at the interface is given by

$$c_i = \frac{M_v}{M_g p / p_v(T_i) - (M_g - M_v)}, \tag{25}$$

where M denotes the molecular weight, and $p_v(T_i)$ the vapor pressure is available from thermodynamic tables.

On the non-wetted wall at $x < X_c$, there occurs no condensation, and thus the mass conservation yields the following condition at the wall,

$$\frac{\partial c}{\partial y^*} = 0. \tag{26}$$

Consequently the problem is reduced to solving the equations (13), (14), (15) so as to satisfy the boundary condition: (18), (19), and (26) for non-wetted region and (18)-(25) for wetted region, respectively. These conditions are rewritten in the dimensionless forms with the assumption of thin liquid layer as,

$$y = 0; \quad U = 0, \quad \theta = \theta_w, \tag{27}$$

$$y \to \infty; \quad U \to 1, \quad \theta \to 1, \quad c \to c_e, \tag{28}$$

$y = \delta$;

$$U = U_L = U_i, \quad \theta = \theta_L = \theta_i, \tag{29}$$

$$A_x \frac{\partial U}{\partial \eta} = \frac{\mu_L}{\mu_i} \frac{dU}{dy}, \tag{30}$$

$$A_x \frac{\partial \theta}{\partial \eta} = \frac{k_L}{k_i} \frac{d\theta}{dy} - Re \cdot Pr h_L \dot{m}, \tag{31}$$

where

$$A_x=\rho_i/\rho_e\cdot\sqrt{Re/2x}\,,\quad Pr=\mu_e C_{p,i}/k_i\,,$$
$$h_L=h_L^*/C_{p,e}T_e\,,\qquad \dot{m}=\dot{m}^*/\rho_e u_e\,.$$

As for the surface conditions for vapor mass fraction, we have

$$0\leqq x<X_c,\ y=0;\ \frac{\partial c}{\partial\eta}=0, \tag{32}$$

$$\left.\begin{aligned} x\geqq x_c,\ y=\delta;\ \frac{A_x}{S_c(1-c_i)}\frac{\partial c}{\partial\eta}&=\frac{d}{dx}\int_0^\delta\frac{\rho_L}{\rho_e}U_L dy\equiv\dot{m}\,,\\ c&=c_i\,, \end{aligned}\right\} \tag{33}$$

where

$$S_c=\mu_e/\rho_i D_i\,.$$

3. Computational method

3.1 Finite difference schemes

We conveniently divide the whole region into three regions: I) the non-wetted wall region, II) the wetted wall region from the film initiation down to a moderate downstream, and III) further downstream region.

It follows from the solution of Eq. (14) with the wall condition (32) that for the region I the vapor mass fraction c is constant across the gas-phase boundary layer. Thus, it suffices to deal with the momentum and energy equations alone. For this region we apply the Hartree-Womersley method modified by Smith et al. [*12*]. This method leads an accurate solution without any specification for the initial profiles of flow variables at the leading edge.

In the region II, the liquid film initiates to grow up toward downstream; i. e. the diffusion layer begins to grow up from the point $x=X_c$ along the film. Therefore, the *H-W* method is still appropriate to the numerical analysis of the diffusion layer in this region. However the *H-W* method is not necessarily appropriate to evaluation of the momentum and thermal boundary layers, because of the complexity in matching of the gas phase solution with that of the liquid layer. To circumvent this complexity, a standard explicit difference scheme is applied to the analysis of the momentum and the thermal boundary layers, which are growing up comparatively thicker in this region. In this paper, the standard explicit scheme is applied; the η-wise derivatives are represented by the central finite difference approximation. In application of the *H-W* method to the diffusion layer remaining variables, U, f, ρ, and D involved in the species conservation equation (14), are specified by the interpolation from the velocity and the temperature profiles evaluated from the standard explicit scheme. The region II is terminated at the location where the diffusion layer becomes as

thick as the momentum and thermal boundary layers.

In the region III after the region II, the streamwise variation in flow variables becomes comparatively small. Therefore, for analysis of region III it is more efficient for computation to use the finite difference scheme proposed by DuFort and Frankel [*13*], being much favorable for the stability of computation. The details of the finite difference scheme employed in the region III should be referred to Appendix.

3.2 Matching procedure

In analysis of the wetted region, the matching procedure of the gas-phase solution with the liquid film solution should be made so as to satisfy the boundary conditions (29)-(31), and (33) at the interface. By the use of the two-point finite difference appoximation, the left hand sides of (30), (31) are expressed at the $(I+1)$ th step in ΔX as

$$\frac{\partial U}{\partial \eta}=\frac{U_{I+1,2}-U_i}{\Delta \eta}, \quad \frac{\partial \theta}{\partial \eta}=\frac{\theta_{I+1,2}-\theta_i}{\Delta \eta}, \tag{34}$$

where

$$U_i=U_{I+1}(J=1), \quad \theta_i=\theta_{I+1}(J=1).$$

Here $\Delta\eta$ is the grid size and the subscripts I and J denote the grid indices for the quantities at the coordinates

$$x=\sum_{I=1}^{I}\Delta X_I, \quad \eta=(J-1)\cdot\Delta\eta.$$

Then with the aid of Eq. (34), and by substituting (16), (17) into (30), (31), respectively, we have the following set of algebraic equations for the unknowns U_i, θ_i, δ, and $\dot{m}$:

$$U_{I+1,2}-U_i=\left(\frac{U_i}{\delta}-GReA\delta\right)\frac{\Delta\eta}{A_x}\frac{\mu_L}{\mu_i}, \tag{35}$$

$$\theta_{I+1,2}-\theta_i=\left(\frac{\theta_i-\theta_w}{\delta}\frac{k_L}{k_i}-RePrh_L\dot{m}_{I+1}\right)\frac{\Delta\eta}{A_x}. \tag{36}$$

In making the two-point finite difference approximation for the x-wise derivative in Eq. (33), the condensation rate is expressed as

$$\dot{m}_{I+1}=\left\{\left[\int_0^\delta\frac{\rho_L}{\rho_e}U_L dy\right]_{I+1}-\left[\int_0^\delta\frac{\rho_L}{\rho_e}U_L dy\right]_I\right\}\Big/\Delta X_{I+1}.$$

The substitution of liquid layer solution (16) into the above equation gives the following algebraic from

$$\left[\frac{\rho_L}{2\rho_e}\left(U_i\delta-\frac{A}{3}GRe\delta^3\right)\right]_{I+1}=\dot{m}_{I+1}\cdot\Delta x_{I+1}+\left[\int_0^\delta\frac{\rho_L}{\rho_e}U_L dy\right]_I. \tag{37}$$

The matching procedure for U_i, θ_i, and $\dot{m}$ is performed as follows:

1. For $\dot{m}_{I+1}$ appropriately chosen we evaluate U_i, θ_i and δ using (35), (36),

and (37).

2. The c_i is evaluated using Eq. (25) with p_v for θ_i above obtained.
3. The species continuity (14) is solved by the H-W method for this c_i. The solution gives $(\partial c/\partial\eta)_i$, and thus $\dot{m}_{I+1}$ is evaluated from Eq. (33).

The procedure above described was iteratively repeated until the deviation of the re-evaluated $\dot{m}_{I+1}$ from the previously attains less than 1×10^{-3}.

For region III instead of step 3 the new value of $\dot{m}_{I+1}$ is obtained from the following difference form of Eq. (33);

$$\dot{m}_{I+1}=\frac{1}{1-c_i}\frac{c_{I+1,2}-c_i}{S_c\Delta\eta}\frac{A_x}{Re}. \tag{38}$$

The diffusion layer as the momentum and thermal boundary layers are analyzed by means of DuFort-Frankel scheme (see Appendix)

3.3 Propriety of the method

The gas-phase boundary layer flow accompanying with the film condensation has a similar feature to the boundary layer flow along a wall with suction. To examine the applicability of the numerical method here proposed, therefore we applied this method to the problem of the boundary layer over a flat plate with suction. The problem is quite the same as one for which the exact similar solution was obtained by Emmons and Leigh [14].

We assume a physical model that the wall is impermeable at $x<X_c$ and the suction is distributed with the suction velocity $v_w\sim1/\sqrt{x}$ along the wall at $x\geqq X_c$. For the case of small wall mass flux, Libby [*10*] presented an expression for the deviation of stream fuction from the similar solution [*14*]

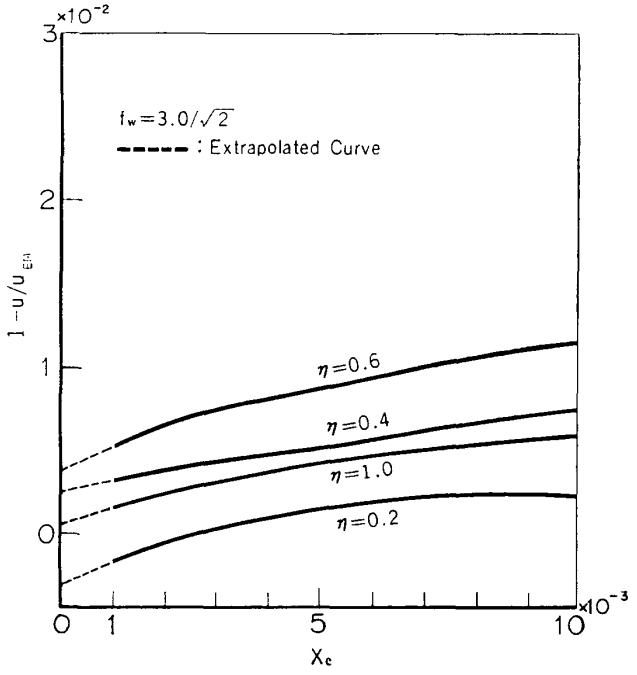

FIG. 2. Velocity data computed for the boundary layer problem with surface suction.

by the power series in terms of the impermeable length X_c. It was confirmed that the solution approaches closely to the similar solution [*14*] with decreasing impermeable length. We examine here the validity of the extrapolation method, which provides the solution for $X_c \to 0$, in the case of comparatively large flux $f_w > 1$; f_w is the dimensionless stream function at the wall.

For this problem we have the Blasius solution for $x < X_c$ and thus the momentum equation (without body force term) concerned has been solved by the standard explicit scheme at $x \geqq X_c$. The computation was performed for the various suction parameters f_w ranging from $0.1/\sqrt{2}$ to $5.0/\sqrt{2}$.

For each suction parameter, the location X_c of suction initiation is chosen as $X_c = 0.001$, 0.005, and 0.01. In Fig. 2 the variation of the dimensionless streamwise velocity at $x = X_c + 0.02$ is expressed by $1 - U/U_{EM.}$ and plotted against X_c for fixed η's; $U_{EM.}$ denotes the results for $X_c = 0$ obtained by Emmons and Leigh [*14*]. The solution for $X_c \to 0$ was evaluated from the extrapolation of the solutions for various finite X_c's. The deviation of the results thus obtained from the exact solution [*14*] is found to be less than 2%. Therefore the extrapolation procedure proposed here is expected to provide a reasonably accurate solution for the suction problem as well as the condensation problem.

4. Results and discussions

4. 1 Flow parameters for computation

Numerical solutions of the boundary layer problem in steam-air mixture undergoing forced flow along a vertical surface was obtained by the aforementioned numerical method. The solutions for several X_c's were obtained for the free stream velocity of 1 fps, 10 fps, and 100 fps for the steam mass fraction c_e of 0.9, 0.09, 0.99, and 0.999 and for the temperature difference $(T_e - T_w)$ ranging from 5 to 36 deg F, with the specified temperature level $T_e = 212$ deg F. The reference length L was chosen as 0.5 ft.

With reference to the proposal by Denny and Mills [*15*], the properties of water were assumed to be the locally constans which can be evaluated at the reference temperature T_r given by

$$T_r = T_w + 0.33(T_i - T_w). \tag{39}$$

For the steam-air mixture concerned, the viscosity, the conductivity, and the diffusion coefficient were evaluated from the data listed in Hilsenrath et al. [*16*], by the use of the mixture rule described in Mason and Monchik [*17*].

4. 2 Accuracy of numerical results

From consideration of truncation error the grid size $\Delta\eta$ was taken as 0.1 with $\eta_e = 7.0$ at the outer edge of the boundary layer. For the case of small x-wise velocity it was tolerable to choose the larger grid size $\Delta\eta$, say 0.2.

The marching step size was chosen as follows. For the region I, the number of steps were ranged from 2 to 20, depending on the magnitude of X_c. At each x-step the solutions were obtained such that deviation from

the uniform stream condition at $\eta_e=7.0$ is less than the accumulated error caused by the *R-K-G* program employes in the *H-W* method. For the region II, the step size Δx was chosen so as to satisfy the Karplus' Criterion [*18*] at each step. The region III was divided into about 300 steps with varying step size for which the truncation errors were less than 0.1%. The resulting accuracy of computation is estimated to be within 0.1% or so.

4. 3 Boundary layers in the vapor-gas mixture

As an example the the profiles of vapor mas fraction and velocity are shown to illustrate the flow near the film initiation point in Figs. 3 and 4, respectively. Figure 3 shows the development of diffusion layer along the film. The concentration gradient $\partial c/\partial\eta$ at the film surface sharply decreases toward downstream near the film initiation point $x=X_c$. From Fig. 4 we can observe a sudden reduction of boundary layer thicknes just behind the film initiation point $x=X_c$; this is caused by the momentum transfer towards the film, being accompanied by the condensing vapor. At moderate downstream the recovery of the thickness of momentum boundary layer can be seen; this is partly attributed to the decrease in condensation rate.

The velocity profiles for the case of $u_e=10$ fps and for the case of $u_e=1$

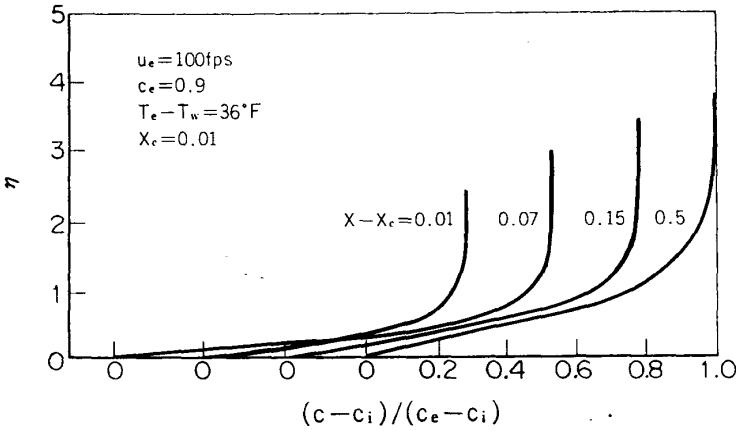

FIG. 3. Profiles of steam mass fraction.

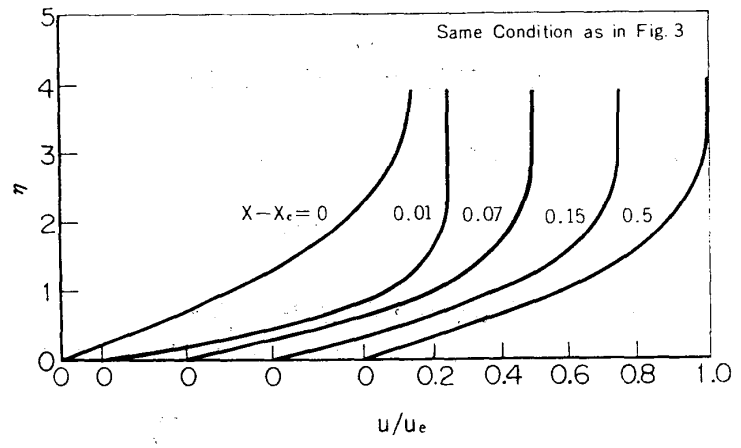

FIG. 4. Velocity profiles $u_e=100$ fps.

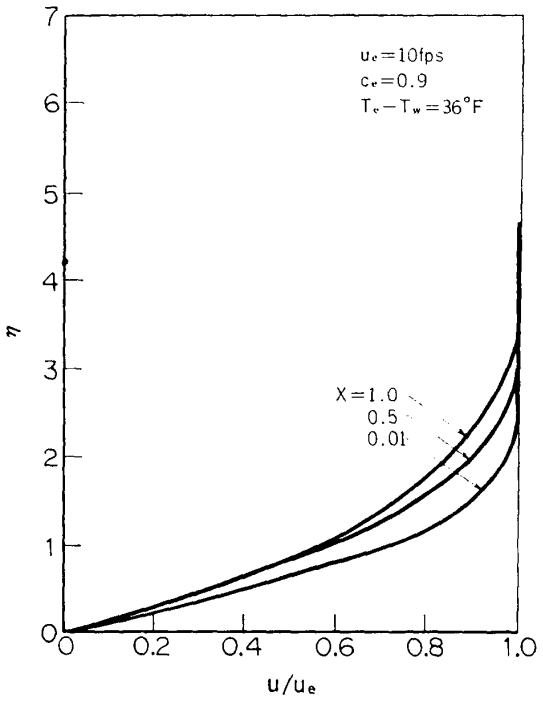

FIG. 5. Velocity profiles $u_e=10$ fps.

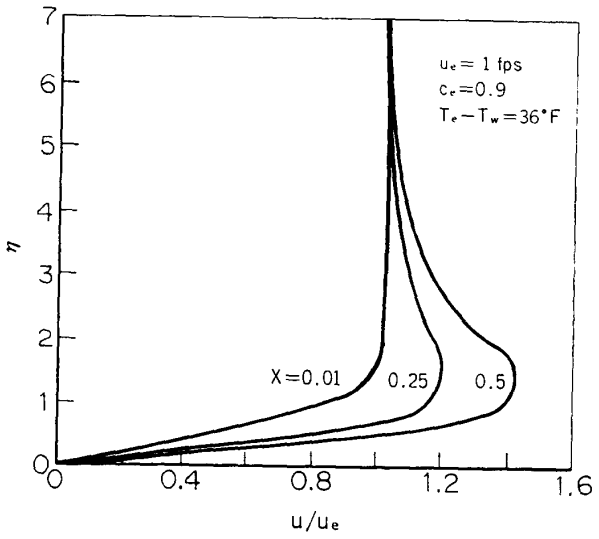

FIG. 6. Velocity profiles $u_e=1$ fps.

are shown in Fig. 5 and Fig. 6, respectively. The velocity profiles for the cases of $u_e=10$ fps is similar to that for the case of $u_e=100$ fps. On the contrast to these cases in the case of $u_e=1$ fps the flow near the film is accelerated over the free stream velocity because of dominant body force.

4.4 Effect of starting-length on the heat transfer

Let introduce the dimensionless wall heat flux q/q_{Nu} where q_{Nu} is the wall heat flux obtained from the classical Nusselt model analysis. With the liquid properties evaluated at the reference temperature T_r given by (39), q_{Nu} is expressed as follows [*1*]:

$$q_{Nu}=\left[\frac{C_{p,L}(T_e-T_w)}{P_{r,L}h_L^*}\right]^{3/4}\left(\frac{g\rho_L^2\mu_L^2}{4x^*}\right)^{1/4}h_L^*. \tag{40}$$

In Fig. 7 the heat transfer q/q_{Nu} is plotted against $x-X_c$ for various X_c's. As mentioned before the limiting values of q/q_{Nu} as $X_c\to 0$ were estimated by a simple extrapolation from the results for finite X_c's. We can see from this figure that the ratio q/q_{Nu} is nearly constant over the region near the rear edge $x=1$ for each X_c's. Therefore the ratio $q/q_{Xc\to 0}$ at the rear edge $x=1$ provides a measure of the effect of the starting-length on the heat

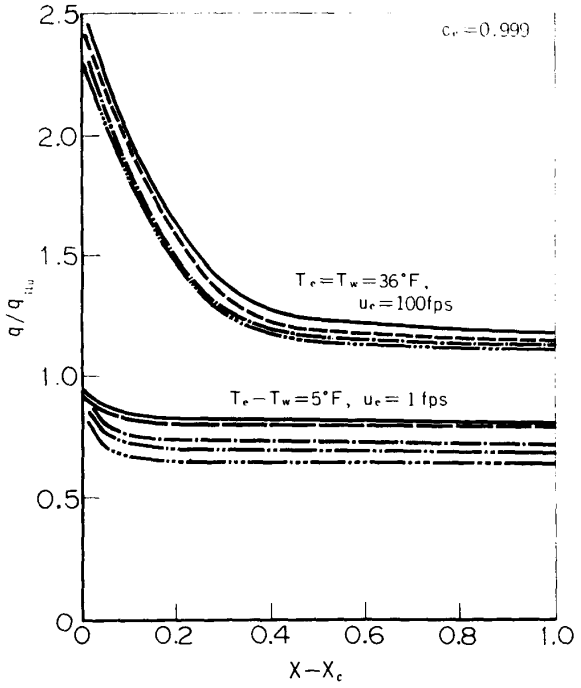

FIG. 7. Heat transfer variation with the starting-length X_c as a parameter. $C_e=0.999$:
——, $X_c=0.001$; — — —, $X_c=0.005$; - - - - -, $X_c=0.01$;
— · — ·, $X_c=0.02$; — · — · —, $X_c=0.05$; — · — · — · —, $X_c=0.1$.

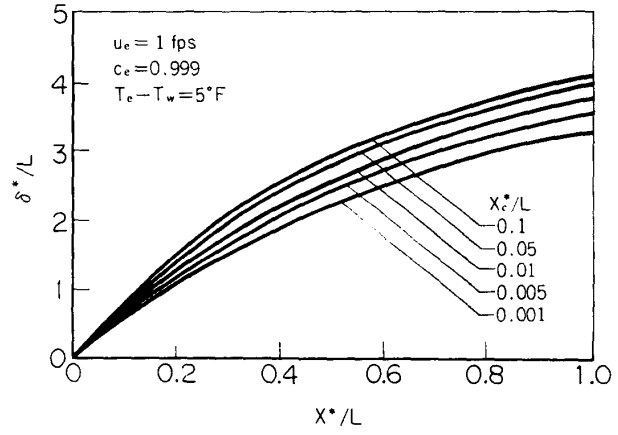

FIG. 8. Dependence of film thickness on assumed location of film initiation.

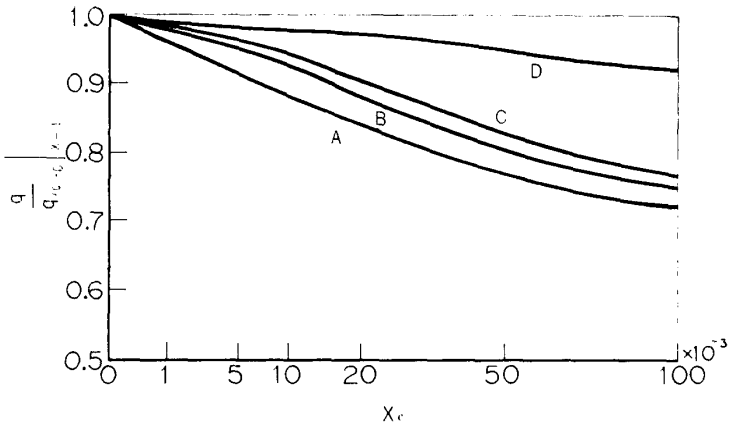

FIG. 9. Effect of $\dot{m}\sqrt{Re}$ on the heat transfer ratio $q/q_{Xc\to 0}$ at the rear edge.

TEBLE 1

	A	B	C	D
$\dot{m}\sqrt{Re}$	8.64	10.4	11.7	23.6
u_e [fps]	10	1	10	1
$T_e - T_w$ [deg F]	36	36	36	20
C_c	0.9	0.999	0.99	0.999

transfer; $q_{Xc\to 0}$ denotes the value of q for the vanishing starting length $X_c \to 0$. Sampling data of the film thickness are plotted in Fig. 8 which shows that for smaller X_c the liquid film is relatively thin.

To clarify the starting-length on heat transfer, we plot the heat tranfer ratio $q/q_{Xc\to 0}|_{x=1}$ in Fig. 9. As naturally expected, the ratio $q/q_{Xc\to 0}|_{x=1}$ decreases with increasing starting-length X_c or with increasing length of non-wetted leading section. It can be shown from a simple dimensional analysis that the ratio of the momentum driven by condensation to the dissipated momentum is measured by the magnitude of $\dot{m}\sqrt{Re}$; although the $\dot{m}\sqrt{Re}$ varies along the liquid surface, as a measure the value at $x = X_c + 0.02$ is tabulated in Table 1 with the flow parameters. From physical point of view it is suggested that for the greater $\dot{m}\sqrt{Re}$ the existence of the non-wetted region less affects the behavior of the flow over the following wetted region. In fact we can see from Fig. 9 with reference to Table 1 that for smaller $\dot{m}\sqrt{Re}$ the decrease in $q/q_{Xc\to 0}|_{x=1}$ is much appreciable with increasing X_c, while for greater $\dot{m}\sqrt{Re}$ $q/q_{Xc\to 0}|_{x=1}$ indicates a weak dependence on X_c.

4.5 Comparison with other analyses

Most of the previous analyses dealt with the flow model that the film initiation occurs just at the leading edge. Recently the case of mixed convection, with which the present analysis is also concerned, was numerically

analyzed by Denny, Mills, and Jusionis [3] by means of an implicit finite difference method. As for difference of the present analysis from the analysis by Denny et al. [3], the type of the numerical scheme is not the subject to be noteworthy, but the following should be noted. The starting-length method proposed here does not require any additional approximation, say an asymptotic shear expression made in the analysis by Denny et al. at the leading edge. Comparison of the present results for $X_c \to 0$ with those by Denny et al. [3] is made in Fig. 10. We can see from the figure an apparent contrast that the heat transfer ratio q/q_{Nu} predicted by the present method asymptotically approaches a nearly constant value as one proceeds

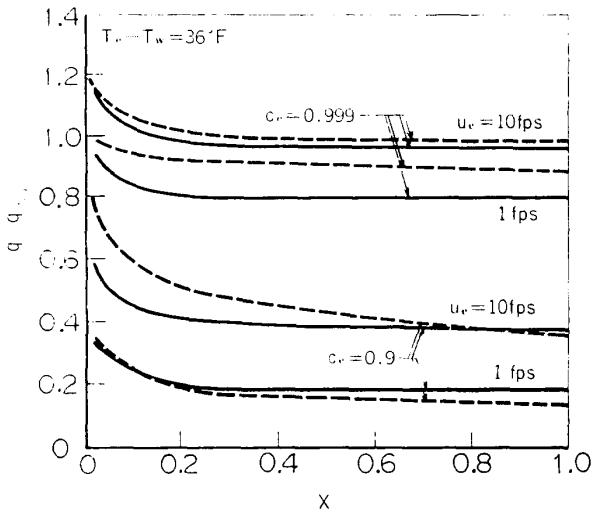

FIG. 10. Comparison with others' results for the case of mixed convection. ——, present method ($X_c \to 0$); – – –, Denny et al.

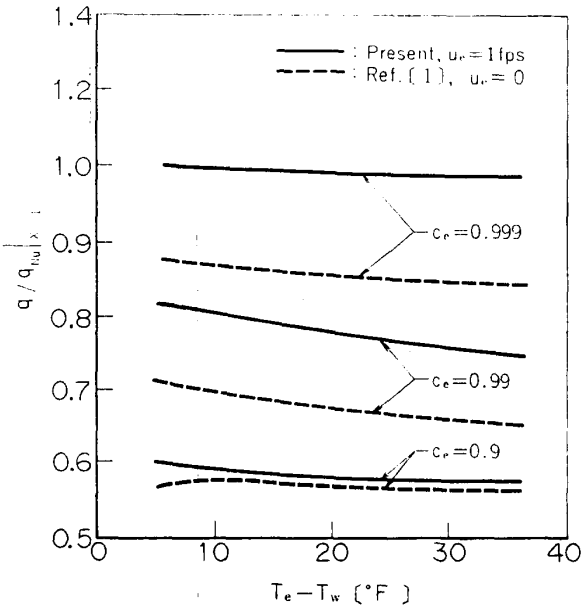

FIG. Comparison with others' resuls for the limiting case.

toward downstream, while the data by Denny et al. [3] do not clearly indicate such a trend. This asymptotic behavior of q/q_{Nu} with increasing x, which is shown in the present results, is likely to be reasonable in view of the fact that at far downstream the effect of body force prevails over the effect of the forced convection. As can be seen from Fig. 7 and 10, for the range $u \lesssim 10$ fps the magnitude of q/q_{Nu} for any x, except for small x, is roughly close to q/q_{Nu} at $x=1.0$.

The comparison of the present results for the mixed convection is made with the results of the analysis for the limiting case of the body force only [1]. For the case of $u_e=1$ fps the $q/q_{Nu}|_{x=1}$ is plotted against the temperature difference T_e-T_w in Fig. 11. In this figure the deviation of the present results from those for the case of body force only [1] shows the effect of the free stream velocity. For the case of $u_e=1$ fps the behavior of $q/q_{Nu}|_{x=1}$ is well analogous to that for the case of body force only [1]. Thus we conclude that in the range $u_e \lesssim 1$ fps the condensation is predicted by the results for the case of $u_e=0$ fps or the case of body force only.

5. Concluding remarks

We presented a numerical analysis of the laminar boundary layer over a condensate film flowing down a vertical flat plate with the non-wetted leading section; as the limiting case, the solution is obtained for the case of vanishing non-wetted section or wholly wetted wall. Finally emphasis is

TEBLE 2 $q/q_{Nu}|_{x^*/L}=1.0$; $L=0.5$ ft, $Te=212$ °F.

$Ce=0.9$

$Te-Tw$ [°F] \ u_e	100 fps	10 fps	1 fps	0.1 fps
5	0.792	0.521	0.206	0.162
20	0.484	0.391	0.187	
36	0.462	0.295	0.163	

$Ce=0.99$

$Te-Tw$ [°F] \ u_e	100 fps	10 fps	1 fps
5	1.132	0.931	0.630
20	1.153	0.879	0.608
36	1.175	0.861	0.569

$Ce=0.999$

$Te-Tw$ [°F] \ u_e	100 fps	10 fps	1 fps
5	1.204	0.9805	0.8310
20	1.221	0.9810	0.8311
36	1.250	0.9831	0.8312

made on the followings,

1) The streamwise variation in flow variables is appreciably large in a narrow region behind the film initiation point. The flow behavior at this region is likely to affect on the flow following toward downstream. Therefore, any assumptions or approximations made for the flow variables at the film initiation point should be minimized in order to clarify the the real flow feature. In view of this this fact, the starting-length method proposed here is much favorable compared with the previous analyses.

2) As regards the heat transfer, it takes the different value depending on the length of non-wetted section not only near the film intiation point $x=X_c$ but also at the rear edge of the plate. The difference is much appreciable for the cases of smaller $\dot{m}\sqrt{Re}$; the ratio of the momentum driven by condensation to the dissipated momentum. In other words for smaller $\dot{m}\sqrt{Re}$ the ratio $q/q_{Xc\to 0}|_{x=1}$ largely varies depending on the length of non-wetted section, while for greater $\dot{m}\sqrt{Re}$ it is less sensitive to the length of non-wetted region.

3) The ratio q/q_{Nu} asymptotically approaches a nearly constant value as one proceed toward downstream, so long as the free stream velocity is not so large; This asymptotic value provides a useful measure to estimate the heat transfer (see Table 2).

The author wishes to acknowledge Professor Hakuro Oguchi for his helpful advices and stimulating discussions throughout this investigation.

Department of Aeronautics
Institute of Space and Aeronautical Science,
University of Tokyo, Tokyo
January 10, 1976

Appendex

The boundary layer is divided with a grid of size $\Delta\eta$ and ΔX with

$$x=\sum^{I}\Delta X_I \quad \text{and} \quad \eta=(J-1)\cdot\Delta\eta.$$

It is assumed that the dependent variable ϕ is known at the grid points in the I-th column and unknown in the $(I+1)$th column.

In the DuFort-Frankel scheme, the x-wise derivative is expressed in the form

$$\left.\frac{\partial\phi}{\partial x}\right|_{I,J}=\frac{\phi_{I+1,J}\Delta X_I-\phi_{I-1,J}\cdot\Delta X_{I+1}}{\Delta X_I+\Delta X_{I+1}}, \tag{A1}$$

where $\Delta x_I=x_I-x_{I-1}$ and $\Delta x_{I+1}=x_{I+1}-x_I$.

Here the subscripts I and J denote the grid indices. The first-order derivative normal to the interface is approximated by central finite difference, and the second-order derivative is expressed in the form

$$\left.\frac{\partial^2\phi}{\partial\eta^2}\right|_{I,J}=\frac{\phi_{I,J+1}+\phi_{I,J-1}-\frac{1}{s}(\phi_{I+1,J}\Delta X_1+\phi_{I-1,J}\Delta X_{I+1})}{\Delta\eta^2}, \tag{A2}$$

where $s=(\Delta X_I+\Delta X_{I+1})/2$.

Applying the difference approximation (A1) and (A2) to the conservation equations (13), (14), and (15), after some manipulation we obtain the following difference expressions for the unknowns $U_{I+1,J}$, $C_{I+1,J}$, and $\theta_{I+1,J}$:

$$\phi_{I+I,J}=\frac{2s}{(U_{I,J}+2\cdot CR)\,\Delta X_I}\left\{CR\left(\phi_{I,J+1}+\phi_{I,J1}-\frac{\Delta X_{I+1}}{s}\varphi_{I-1,J}\right)\right.$$
$$\left.+\frac{U_{I,J}\cdot\phi_{I-1,J}\cdot\Delta X_{I+1}}{2s}+\frac{\phi_{I,J+1}-\phi_{I,J-1}}{2\Delta\eta}\left(\frac{f_{I,J}-f_{I,J-1}}{\Delta X_1}+\frac{f_{I,J}}{2x}+CM\right)+F\right\}$$

where

$$CR=\frac{R_{I,J+1}+R_{I,J-1}}{4x\Delta\eta^2},\qquad CM=\frac{R_{I,J+1}-R_{I,J-1}}{4x\Delta\eta},$$

$$f_{I,J}=f_{I,J-1}+(U_{I,J}+U_{I,J-1})\frac{\Delta\eta}{2}.$$

In the above expression $R_{I,J}$ and F are represented in calculation of each unknown $U_{I+1,J}$, $c_{I+1,J}$, or $\theta_{I+1,J}$ as follows:

$$\phi=U;\quad F=G\left(1-\frac{\rho_e}{\rho_{I,J}}\right),\qquad R_{I,J}=\frac{[\rho\mu]_{I,J}}{\rho_e\mu_e},$$

$$\phi=c;\quad F=0,\qquad R_{I,J}=\frac{[\rho^2D]_{I,J}}{\rho_e\mu_e},$$

$$\phi=\theta;\quad F=\frac{\theta_{I,J+1}-\theta_{I,J-1}}{4x\Delta\eta}\frac{C_{p,v}-C_{p,g}}{C_{p_{I,J}}}\frac{[\rho^2D]_{I,J}}{\rho_e\mu_e}\frac{C_{I,J+1}-C_{I,J-1}}{2\Delta\eta},$$

$$R_{I,J}=\frac{[\rho k/C_p]_{I,J}}{\rho_e\mu_e}.$$

References

[1] W. J. Minkowycz and E. M. Sparrow: Int. J. Heat Mass Transfer **9**, 1125 (1966).
[2] E. M. Sparrow, W. J. Minkowycz and M. Saddy: Int. J. Mass Heat Transfer **10**, 1829 (1971).
[3] V. E. Denny, A. F. Mills and V. J. Jusionis: Trans. ASME, J. Heat Transfer **93**, 297 (1971).
[5] E. R. G. Eckert: *Introduction to the Transfer of Heat and Mass*, 1st Ed. (Mcgraw-Hill Press, New York, 1950), Chap. 7.
[5] M. J. Lighthill: Proc. Roy. Soc. **A202**, 359 (1950).
[6] S. Scesa and S. Levy: Trans. ASME **76**, 759 (1954).
[7] H. Fox and P. A. Libby: J. Fluid Mech. **19**, 433 (1964).
[8] S. C. Cheng, L. C. Birta, and Y. L. Su: Int. J. Heat Mass Transfer **15**. 1933 (1972).

[9] E. R. G. Eckert: VDI-Forschungsheft **416** (1942).
[*10*] P. A. Libby: Int, J. Heat Mass Transfer **9**, 1109 (1966).
[*11*] W. Nusselt: Z. Ver. Dt. Ing. 60, 541 (1916).
[*12*] A. M. O. Smith and N. A. Jaffe: A. I. A. A. J. 8, 193 (1966).
[*13*] E. C. DuFort and S. P. Frankel: Mathematical Tables Aids Computation **7**, 135 (1953).
[*14*] H. W. Emmons and D. C. Leigh: Aeronaut. Res. Coun., Report No. FM 1915 (1958).
[*15*] V. E. Denny and A. F. Mills: Int. J. Heat and Mass Transfer **12**, 965 (1969).
[*16*] J. Hilsenrath, C. W. Beckett et al.: *Tables of Thermodynamic and Transport properties of Gases* (Pergamon Press, London, 1960).
[*17*] E. A. Mason and L. Monchic: J. Chem. Phys. **36**, 2747 (1962).
[*18*] W. J. Karplus: Trans. A. I. E. E. **77**, 210 (1958).